Inorg. Chem. **2009**, *48*, 4569−4579

Catalase vs Peroxidase Activity of a Manganese(II) Compound: Identification of a Mn(III)−(μ-O)$_2$−Mn(IV) Reaction Intermediate by Electrospray Ionization Mass Spectrometry and Electron Paramagnetic Resonance Spectroscopy

Josane A. Lessa,[†] Adolfo Horn, Jr.,[†] Érika S. Bull,[†] Michelle R. Rocha,[†] Mario Benassi,[‡] Rodrigo R. Catharino,[‡] Marcos N. Eberlin,[‡] Annelise Casellato,[§] Christoper J. Noble,[§,||] Graeme R. Hanson,[||] Gerhard Schenk,[§] Giselle C. Silva,[⊥] O. A. C. Antunes,[⊥] and Christiane Fernandes*[,†]

Laboratório de Ciências Químicas, Universidade Estadual do Norte Fluminense, 28013-602, Campos dos Goytacazes, RJ, Brazil, Laboratório ThoMSon de Espectrometria de Massas, Instituto de Química, Universidade Estadual de Campinas, 13084-971, Campinas, SP, Brazil, School of Chemistry and Molecular Biosciences, The University of Queensland, St. Lucia, QLD 4072, Australia, Centre for Magnetic Resonance, The University of Queensland, St. Lucia, QLD 4072, Australia, and Instituto de Química, Universidade Federal do Rio de Janeiro, CT Bloco A, Laboratory. 641, Cidade Universitária, 21945-970, Rio de Janeiro, RJ, Brazil

Received October 15, 2008

Herein, we report reactivity studies of the mononuclear water-soluble complex [Mn(II)(HPClNOL)(η_1-NO$_3$)(η_2-NO$_3$)] **1**, where HPClNOL = 1-(bis-pyridin-2-ylmethyl-amino)-3-chloropropan-2-ol, toward peroxides (H_2O_2 and *tert*-butylhydroperoxide). Both the catalase (in aqueous solution) and peroxidase (in CH_3CN) activities of **1** were evaluated using a range of techniques including electronic absorption spectroscopy, volumetry (kinetic studies), pH monitoring during H_2O_2 disproportionation, electron paramagnetic resonance (EPR), electrospray ionization mass spectrometry in the positive ion mode [ESI(+)-MS], and gas chromatography (GC). Electrochemical studies showed that **1** can be oxidized to Mn(III) and Mn(IV). The catalase-like activity of **1** was evaluated with and without pH control. The results show that the pH decreases when the reaction is performed in unbuffered media. Furthermore, the activity of **1** is greater in buffered than in unbuffered media, demonstrating that pH influences the activity of **1** toward H_2O_2. For the reaction of **1** with H_2O_2, EPR and ESI(+)-MS have led to the identification of the intermediate [Mn(III)Mn(IV)(μ-O)$_2$(PClNOL)$_2$]$^+$. The peroxidase activity of **1** was also evaluated by monitoring cyclohexane oxidation, using H_2O_2 or *tert*-butylhydroperoxide as the terminal oxidants. Low yields (<7%) were obtained for H_2O_2, probably because it competes with **1** for the catalase-like activity. In contrast, using *tert*-butylhydroperoxide, up to 29% of cyclohexane conversion was obtained. A mechanistic model for the catalase activity of **1** that incorporates the observed lag phase in O_2 production, the pH variation, and the formation of a Mn(III)−(μ-O)$_2$−Mn(IV) intermediate is proposed.

Introduction

Oxygen, though essential for aerobic metabolism, can be converted to toxic metabolites, such as the superoxide anion, hydroxyl radical, and hydrogen peroxide, collectively known as reactive oxygen species (ROS). These ROS are associated with numerous pathological conditions including ischemic and inflammatory processes.[1] All living cells therefore use exquisitely orchestrated mechanisms to control the level of ROS, including the use of endogenous antioxidant metal-

* To whom correspondence should be addressed. E-mail: chrisf@uenf.br. Fax: + 55 22 2739 7046. Phone: + 55 22 2739 7158.
[†] Universidade Estadual do Norte Fluminense.
[‡] Universidade Estadual de Campinas.
[§] School of Molecular and Microbial Sciences, The University of Queensland.
[||] Centre for Magnetic Resonance, The University of Queensland.
[⊥] Universidade Federal do Rio de Janeiro.

(1) (a) Sies, H. *Angew. Chem.* **1986**, *25*, 1058–1071. (b) Doctrow, S. R.; Huffman, K.; Marcus, C. B.; Tocco, G.; Malfroy, E.; Adinolfi, C. A.; Kruk, H.; Baker, K.; Lazarowych, N.; Mascarenhas, J.; Malfroy, B. *J. Med. Chem.* **2002**, *45*, 4549–4558.

10.1021/ic801969c CCC: $40.75
Published on Web 04/16/2009

loenzymes such as the superoxide dismutases (SODs) and catalases (CATs), which catalyze the dismutation of superoxide and the disproportionation of H_2O_2, respectively.[2] Furthermore, H_2O_2 is employed by heme-containing peroxidases to oxidize various substrates, including organic compounds (phenol), proteins (cytochrome *c*), peptides (glutathione), NADPH, fatty acids. Recently, they have been employed to oxidize dyes and other pollutant compounds.[3] CATs and peroxidases are widespread and protect against the build-up of dangerous concentrations of hydrogen peroxide in living systems, which is formed as a consequence of only partial reduction of dioxygen.[4] However, if the production of H_2O_2 exceeds the capacity of these enzymes, H_2O_2 becomes a substrate for the Fenton reaction, forming the extremely toxic and mutagenic hydroxyl radicals ($OH^{\bullet}$).[5]

While the majority of CATs rely on the heme group for catalysis, an alternative class of manganese-dependent CATs (MnCATs) has been identified in three bacterial organisms: *Lactobacillus plantarum*,[6] *Thermus thermophilus*,[7] and *Thermoleophilum album*.[8] Recent crystallographic studies revealed an elegant structure in which the active sites of the MnCATs from *T. thermophilus* and *L. plantarum* comprise two manganese atoms triply bridged by the carboxylate group of a glutamate and two water-derived ligands.[9] Completing the coordination sphere, each manganese center contains one glutamate and one histidine. Besides the catalytically active Mn_2(II,II) and Mn_2(III,III) oxidation states, the inactive Mn_2(II,III) and Mn_2(III,IV) oxidation states can also be experimentally accessed and transformed into one another via various oxidants and reductants.[10,11]

Although the crystal structures of two MnCATs have been determined, their catalytic mechanism is still a topic of discussion. Most of the mechanistic hypotheses have been based on studies of biomimetic compounds.[11−23] Several types of dinuclear manganese model complexes with catalase activity have been reported but only a few of them proceed via the Mn(II)Mn(II) ↔ Mn(III)Mn(III) redox cycle as observed in the enzymes.[13,14] Dinucleating diamine and diimine ligands have been employed with success in the synthesis of functional models for MnCATs. Among these, the most efficient MnCAT mimic is [Mn(IV)salpn(μ-O)]$_2$ (for salpn and other ligand names: see ref 24) which cycles between $Mn(IV)_2$ and $Mn(III)_2$ oxidation states.[15,16] Usually these ligands present alcohol or phenol groups to help keep the preorganized dinuclear unit in close proximity. Tridentate amines (bpia, Hpda, H_2bpg, tpa)[17−19] have been employed recently in the development of structural and functional MnCAT models.

In attempts to generate complexes that are useful as structural and/or functional models for several metalloenzymes, we successfully used the tripodal ligand 1-(bis-pyridin-2-ylmethyl-amino)-3-chloropropan-2-ol (HPClNOL) (Scheme 1) to form water-soluble complexes.[25−27] This is advantageous as it allows reactivity studies to be performed

(2) (a) Matés, J. M. *Toxicology* **2000**, *153*, 83–104. (b) Benov, L.; Fridovich, I. *J. Biol. Chem.* **1998**, *273*, 10313–10316.

(3) (a) Timofeevski, S. L.; Nie, G.; Reading, N. S.; Aust, S. D. *Arch. Biochem. Biophys.* **2000**, *373*, 147–153. (b) Ürek, R.Ö.; Pazarlioglu, N. K. *Process Biochem.* **2005**, *40*, 83–87.

(4) Haschke, R. H.; Friehoff, J. M. *Biochem. Biophys. Res. Commun.* **1978**, *80*, 1039–1042.

(5) Helliwell, B.; Gutteridge, J. M. C. *Free radicals in biology and medicine*; Clarendon Press:Oxford, U.K., 1989.

(6) (a) Kono, Y.; Fridovich, I. *J. Biol. Chem.* **1983**, *258*, 6015–6019. (b) Beyer, W. F., Jr.; Fridovich, I. *Biochemistry* **1985**, *24*, 6460–6467.

(7) Barynin, V. V.; Hempstead, P. D.; Vagin, A. A.; Antonyuk, S. V.; Melik-Adamyan, W. R.; Lamzin, V. S.; Harrison, P. M.; Artymyuk, P. J. *J. Inorg. Biochem.* **1997**, *67*, 196.

(8) Allgood, G. S.; Perry, J. J. *J. Bacteriol.* **1986**, *168*, 563–567.

(9) (a) Antonyuk, S. V.; Melik-Adamyan, V. R.; Popov, A. N.; Lamzin, V. S.; Hempstead, P. D.; Harrison, P. M.; Artmyuk, P. J.; Barynin, V. V. *Crystallog. Rep. (Transl. Kristallografiya)* **2000**, *45*, 105–116. (b) Barynin, V. V.; Whittaker, M. M.; Antonyuk, S. V.; Lamzin, V. S.; Harrison, P. M.; Artymiuk, P. J.; Whittaker, J. *Structure* **2001**, *9*, 725–738.

(10) (a) Khangulov, S. V.; Barynin, V. V.; Antonyuk-Barynina, S. V. *Biochim. Biophys. Acta, Bioenerg.* **1990**, *1020*, 25–33. (b) Waldo, G. S.; Penner-Hahn, J. E. *Biochemistry* **1995**, *34*, 1507–1512.

(11) Wu, A. J.; Penner-Hahn, J. E.; Pecoraro, V. L. *Chem. Rev.* **2004**, *104*, 903–938. (b) Mukhopadhyay, S.; Mandal, S. K.; Bhaduri, S.; Armstrong, W. H. *Chem. Rev.* **2004**, *104*, 3981–4026.

(12) Dubois, L.; Xiang, D-F.; Tan, X-S.; Latour, J-M. *Eur. J. Inorg. Chem.* **2005**, 1565–1571.

(13) Gelasco, A.; Bensiek, S.; Pecoraro, V. L. *Inorg. Chem.* **1998**, *37*, 3301–3309.

(14) (a) Boelrijk, A. E. M.; Dismukes, G. *Biochemistry.* **1994**, *33*, 15433–15436. (b) Pecoraro, V. L.; Baldwin, M. J.; Gelasco, A. *Chem. Rev.* **1994**, *94*, 807–826, and references therein. (c) Boelrijk, A. E. M.; Dismukes, G. C. *Inorg. Chem.* **2000**, *39*, 3020–3028. (d) Mathur, P.; Crowder, M.; Dismukes, G. C. *J. Am. Chem. Soc.* **1987**, *109*, 5227–5233. (e) Pessiki, P. J.; Khangulov, S. V.; Ho, D. M.; Dismukes, G. C. *J. Am. Chem. Soc.* **1994**, *116*, 891–897. (f) Pessiki, P. J.; Dismukes, G. C. *J. Am. Chem. Soc.* **1994**, *116*, 898–903. (g) Gelasco, A.; Pecoraro, V. L. *J. Am. Chem. Soc.* **1993**, *115*, 7928–7929. (h) Gelasco, A.; Kirk, M. L.; Kampf, J. W.; Pecoraro, V. L. *Inorg. Chem.* **1997**, *36*, 1829–1837. (i) Sasaki, Y.; Akamatsu, T.; Tsuchiya, K.; Ohba, S.; Sakamoto, M.; Nishida, Y. *Polyhedron* **1998**, *17*, 235–242.

(15) (a) Larson, E. J.; Pecoraro, V. L. *J. Am. Chem. Soc.* **1991**, *113*, 3810–3818. (b) Larson, E. J.; Pecoraro, V. L. *J. Am. Chem. Soc.* **1991**, *113*, 7809–7810.

(16) Signorella, S.; Rompel, A.; Buldt-Karentzopoulos, K.; Krebs, B.; Pecoraro, V. L.; Tuchagues, J-P. *Inorg. Chem.* **2007**, *46*, 10864–10868.

(17) Triller, M. U.; Hsieh, W.; Pecoraro, V. L.; Rompel, A.; Krebs, B. *Inorg. Chem.* **2002**, *41*, 5544–5554.

(18) Dubois, L; Pécaut, J.; Carlot, M.-F.; Baffert, C.; Collomb, M.-N.; Deronzier, A.; Latour, J.-M. *Chem.—Eur. J.* **2008**, *14*, 3013–3025.

(19) Shin, B.-K.; Kim, Y.; Kim, M.; Han, J. *Polyhedron* **2007**, *26*, 4557–4566.

(20) Biava, H.; Palopoli, C.; Shova, S.; De Gáudio, M.; Daier, V.; González-Sierra, M.; Tuchagues, J.; Signorela, S. *J. Inorg. Biochem.* **2006**, *100*, 1660–1671.

(21) Dubois, L.; Caspar, R.; Jacquamet, L.; Petit, P.; Charlot, M.; Baffert, C.; Collomb, M.; Deronzier, A.; Latour, J. -M. *Inorg. Chem.* **2003**, *42*, 4817–4827.

(22) Moreno, D.; Palopoli, C; Daier, V.; Shova, S.; Vendier, L.; Sierra, M. G.; Tuchagues, J.-P.; Signorella, S. *Dalton Trans.* **2006**, 5156–5166.

(23) Karsten, P.; Neves, A.; Bortoluzzi, A. J.; Strähle, J.; Maichle-Mössmer, C. *Inorg. Chem. Commun.* **2002**, *5*, 434–438.

(24) H_2salpn = 1,3-bis(salicylideneiminato)-propane; bpia = bis-(picolyl)(*N*-methylimidazol-2-yl)amine; tpa = tris-2-picolyamine, Hbpg = bis-2-picolylglycylamine; H_2pda = 2-picolyldiglycylamine; H_3nta = nitrilo-tris-acetic acid; L^1H_3 = 1,5-bis(2-hydroxybenzophenylideneamino)pentan-3-ol; L^2H_3 = 1,5-bis(2-hydroxynaphthylideneamino)-pentan-3-ol; bmpa = (bis-pyridylmethyl)amine; HL = 2-(bis-(2-pyridylmethyl)aminomethyl)-6-((2-pyridylmethyl)(benzyl)aminomethyl)-4-methylphenol; MPBMPA = *N*-methylpropanoate-*N*,*N*-bis-(2-pyridylmethyl)amine; PBMPA = *N*-propanoate-*N*,*N*-bis-(2-pyridylmethyl)amine; PABMPA = *N*-propanamide-*N*,*N*-bis-(2-pyridylmethyl)amine.

(25) (a) Fernandes, C.; Parrilha, G. L.; Lessa, J. A.; Santiago, L. J. M.; Kanashiro, M. M.; Boniolo, F. S.; Bortoluzzi, A. J.; Vugman, N. V.; Herbst, M. H.; Horn, A. *Inorg. Chim. Acta* **2006**, *359*, 3167–3176. (b) Parrilha, G. L.; Fernandes, C.; Bortoluzzi, A. J.; Szpoganicz, B.; Silva, M. de S; Pich, C. T.; Terenzi, H.; Horn, A. *Inorg. Chem. Commun.* **2008**, *11*, 643–647.

(26) Lessa, J. A.; Horn, A.; Pinheiro, C. B.; Farah, L. L.; Eberlin, M. N.; Benassi, M.; Catharino, R. R.; Fernandes, C. *Inorg. Chem. Commun.* **2007**, *10*, 863–866.

Scheme 1. Synthesis of **1**

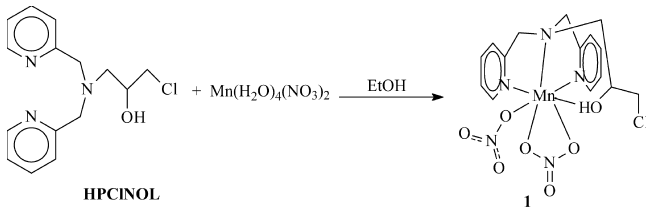

in aqueous solutions. The HPClNOL ligand was employed successfully in the synthesis of copper and iron complexes, which are functional models for nucleases.[25] Here, the HPClNOL ligand was employed to synthesize the mononuclear water-soluble complex [Mn(II)(HPClNOL)(η_1-NO_3)(η_2-NO_3)], **1** (Scheme 1). Characterization of **1** by X-ray diffraction and ESI-(+)-MS(/MS) has been published.[26] In this work, we have evaluated the catalytic ability of **1** to promote H_2O_2 disproportionation using assay conditions similar to those used to determine the kinetic properties of MnCATs. The reaction was monitored by following O_2 evolution, ESI-(+)-MS, EPR, electronic absorption spectroscopy, and following changes in pH. The studies were performed with and without pH control, employing TRIS/TRIS·HCl (TRIS: tris(hydroxymethyl)aminomethane) as buffer. Since the activation of peroxide molecules by metal compounds is of interest for promoting the oxidation of organic molecules (peroxidase activity), we also present data concerning the catalytic ability of **1** in promoting the oxidation of cyclohexane using H_2O_2 and *tert*-butylhydroperoxide (*t*-BuOOH) as oxidants.

Experimental Section

Materials. Dimethylformamide (DMF) was distilled in vacuum and stored under an argon atmosphere prior to electrochemical studies. All the other reagents and solvents were of analytical and/or spectroscopic grade and were used without further purification.

Ligand and Complex Syntheses. The ligand HPClNOL was synthesized by a reaction between the secondary amine bmpa and epichlorohydrin, as reported previously.[27] The mononuclear [Mn(II)-(HPClNOL)(η_1-NO_3)(η_2-NO_3)] complex **1** was prepared according to a published procedure (Scheme 1).[26]

Spectroscopic Methods. UV−vis spectra were recorded in water on a Shimadzu 1601 PC UV−vis spectrophotometer. EPR spectra were recorded on a Bruker Elexsys E580 EPR spectrometer equipped with a Bruker ER036TM Teslameter and frequency counter for calibration of the magnetic field and microwave frequency, respectively. Low temperature (140 K) at the sample position employed a nitrogen flow-through system in conjunction with a liquid nitrogen Eurotherm ER4131vt temperature controller. Experimental conditions were as follows: peroxide titrations were performed in buffered solutions (TRIS/TRIS·HCl, 1.0 mmol·L^{-1}; pH 7.2), and samples were rapidly frozen in liquid nitrogen at specified time intervals. Each experiment was conducted by adding 8 μL of a hydrogen peroxide solution (stock concentrations: 0.55 and 4.4 mol·L^{-1}, respectively) to 180 μL of a 1 mmol·L^{-1} solution of the complex **1**. Computer simulation of the dimanganese EPR spectra employed Molecular Sophe[28] in conjunction with Octave[29] to allow the optimization of the spin Hamiltonian parameters.

ESI-(+)-MS. The experiments were performed using a Q-TOF mass spectrometer (Micromass, Manchester, UK). The ionization technique used was electrospray ionization in the positive ion mode (ESI-(+)-MS). Typical conditions were the following: source and desolvation temperatures of 353 K, and capillary and cone voltages of 3 kV and 40V, respectively. To a solution of **1** (1 mL, 1×10^{-6} mol·L^{-1}, MeOH:H_2O 1:1) was added 50 μL of H_2O_2 (23%) and the reaction was followed over 20 min. The sample was injected using a syringe pump (Harvard Apparatus) at a flow rate of 10 μL·min^{-1}. Mass spectra were acquired over the 50−1500 *m/z* range.

Electrochemistry. Electrochemical studies were performed with an Autolab PGSTAT 10 potentiostat/galvanostat in acetonitrile containing 0.1 M tetrabutylammonium perchlorate ($TBAClO_4$) as the supporting electrolyte under an argon atmosphere at room temperature. The electrochemical cell employed a standard three-electrode configuration: a glassy carbon working electrode, a platinum-wire auxiliary electrode, and a commercial Ag/AgCl electrode immersed in a salt bridge containing 0.1 M $TBAClO_4$. The ferrocene/ferrocenium (Fc/Fc^+) couple (0.400 V vs NHE) was used as an internal standard.[30]

Catalase-like Activity. All the reactions between **1** and H_2O_2 were performed in buffered (TRIS/TRIS·HCl, 0.1 mol·L^{-1}; pH 7.2, $LiClO_4$ 0.1 mol·L^{-1}) and in unbuffered water solutions ($LiClO_4$ 0.1 mol·L^{-1}). Initially, the reactivity of **1** toward H_2O_2 was investigated in water ($LiClO_4$ 0.1 mol·L^{-1}) via UV−vis spectroscopy. A solution of **1** was prepared and was kept at room temperature for 12 h prior to use. Then, 10 μL of H_2O_2 (21%) was added to the aqueous solution of the complex (5×10^{-3} mol·L^{-1}, 3 mL), and spectra were recorded at 90 s intervals in a 1 cm path length cell. A similar study was performed using a buffered system (TRIS/TRIS·HCl, 0.1 mol·L^{-1}; pH 7.2, $LiClO_4$ 0.1 mol·L^{-1}).

Volumetric measurements of the evolved dioxygen produced during the reactions of **1** with H_2O_2 were performed in triplicate as follows: a 10 mL round-bottom flask containing an aqueous solution of **1** (1×10^{-3} mol·L^{-1}, 5.00 mL) and $LiClO_4$ (0.1 mol·L^{-1}, 1 mL) was placed in a water bath (298.00 ± 0.01 K). The flask was closed by a rubber septum and a cannula was used to connect the reaction flask to an inverted graduated pipet, filled with water. While the solution containing the complex was being stirred, a solution of H_2O_2 diluted to appropriate concentrations was injected through the rubber septum using a microsyringe. The volume of oxygen produced was measured in the pipet. Experiments were performed keeping the concentration of the substrate constant and varying the concentration of the complex to determine the order with respect to the complex. A similar study was performed to obtain the order with respect to the substrate.

The pH variation during H_2O_2 disproportionation was carried out in triplicate under unbuffered conditions as follows: a flask containing an aqueous solution of the complex (1×10^{-3} mol·L^{-1}, 5.00 mL) and $LiClO_4$ (0.1 mol·L^{-1}, 1 mL) was placed in a water bath (298.00 ± 0.01 K). The pH was determined by using a Micronal model B374 pH meter fitted with an Analion model V631 electrode. A solution of H_2O_2 diluted to appropriate concentration with water was then added to this solution, which was stirred and the pH values were measured at 5 s time intervals.

(27) Horn, A.; Fernandes, C.; Bortoluzzi, A. J.; Vugman, N. V.; Herbst, M. H. J. *Mol. Struct.* **2005**, *749*, 96–102.

(28) Hanson, G. R.; Noble, C. J.; Benson, S. *Biol. Magn. Reson.* **2008**, *28*, 105–174.

(29) Octave v 3.0.1 can be obtained from www.octave.org.

(30) Gagné, R. R.; Koval, C. A.; Lisensky, G. C. *Inorg. Chem.* **1980**, *19*, 2854–2855.

Peroxidase-like Activity. The reactions were performed in a 50 cm^3 round-bottom flask under stirring for 24 h. The catalyst: substrate:oxidant ratio was 1:1000:1000 with the following reagent amounts: 0.75 cm^3 of cyclohexane (7×10^{-3} mol), 0.59 cm^3 of H_2O_2 or 0.93 cm^3 of *t*-BuOOH (7×10^{-3} mol), and 3.3 mg of **1** (7×10^{-6} mol). Acetonitrile (MeCN) and *t*-butanol (*t*-BuOH) were used as solvent (10 cm^3), and the experiments were performed at two temperatures: room temperature (rt) and 50 °C. The reactions were quenched by adding an aqueous 0.4 mol·L^{-1} solution of Na_2SO_4, followed by extraction with 10 cm^3 of diethyl ether. The ether layer was dried with anhydrous Na_2SO_4 and analyzed by GC. The aqueous phase was titrated with NaOH to quantify the total of acid compounds obtained in the reaction expressed as adipic acid.

Results and Discussion

Electrochemical Properties of 1. Results obtained by cyclic and pulse differential voltammetry in DMF (Figure S1, Supporting Information) indicate the presence of two redox processes at 0.65 V ($\Delta E_p = 56$ mV) and 0.92 V ($\Delta E_p = 40$ mV) vs Fc/Fc^+. The processes are attributed to the oxidation of the Mn(II) center to Mn(III) and then to Mn(IV), respectively. These values are shifted to more positive potential with respect to the corresponding redox couple presented by compound $[Mn(III)(bpia)Cl_2](ClO_4)$, which presents processes at $E_{1/2} = 0.61$ V and $E_{1/2} = 1.53$ V vs SCE.[17]

Catalase-like Activity of 1 Measured by UV−vis Spectroscopy. When H_2O_2 is added to a colorless aqueous solution of **1**, it becomes greenish-brown and liberates O_2. The progress of the reaction between **1** and H_2O_2 was monitored in water by UV−vis spectroscopy (Figure 1). Complex **1** shows no absorption features in the visible range, and its unique band in the UV range ($\lambda = 255$ nm, $\varepsilon = 1.2 \times 10^4$ L·mol^{-1}·cm^{-1}) is due to a $\pi \rightarrow \pi^*$ transition involving the pyridine groups of the ligand.[31] This feature is similar to that exhibited by the MnCAT from *T. thermophilus* in the (II,II) oxidation state, which also lacks features in the visible absorption spectrum.[32] Immediately after the addition of 10 μL of H_2O_2 (6.85 mol·L^{-1}) to the aqueous solution (3 mL) of **1** (1×10^{-3} mol·L^{-1}), poorly resolved absorption bands or shoulders near 410, 539, and 620 nm are observed (absorbance = 0.35, 0.11, and 0.083, respectively).[33] Similar absorption bands (three absorption bands between 400−700 nm) were observed when the dimanganese(II,II) complexes $[Mn_2(L)(OAc)_2(CH_3OH)](ClO_4)$ and $[Mn_2(L)(OBz)(H_2O)](ClO_4)$,[21] reported by Latour, were allowed to react with H_2O_2 in acetonitrile. Mn(III)Mn(IV)-di-μ-oxo complexes containing the tripodal ligands bpia,[17] tpa, bpg, and pda[18] also exhibit similar absorption bands. Using the assignment proposed by Solomon *et al.*,[34] the band at highest energy has been assigned to an oxo → Mn(IV) charge-transfer transition (LMCT), while the others (λ = 500−560 nm, λ = 590−600 nm) are related to Mn(IV) d−d transitions. Krebs has proposed that the highest energy band also has a d−d contribution while the lowest energy band is related to a LMCT oxo → Mn(IV).[17] Thus, the presence of similar absorption bands in **1**, upon the addition of H_2O_2, suggests that a [Mn(III)−(μ-O)$_2$−Mn(IV)] intermediate is formed.

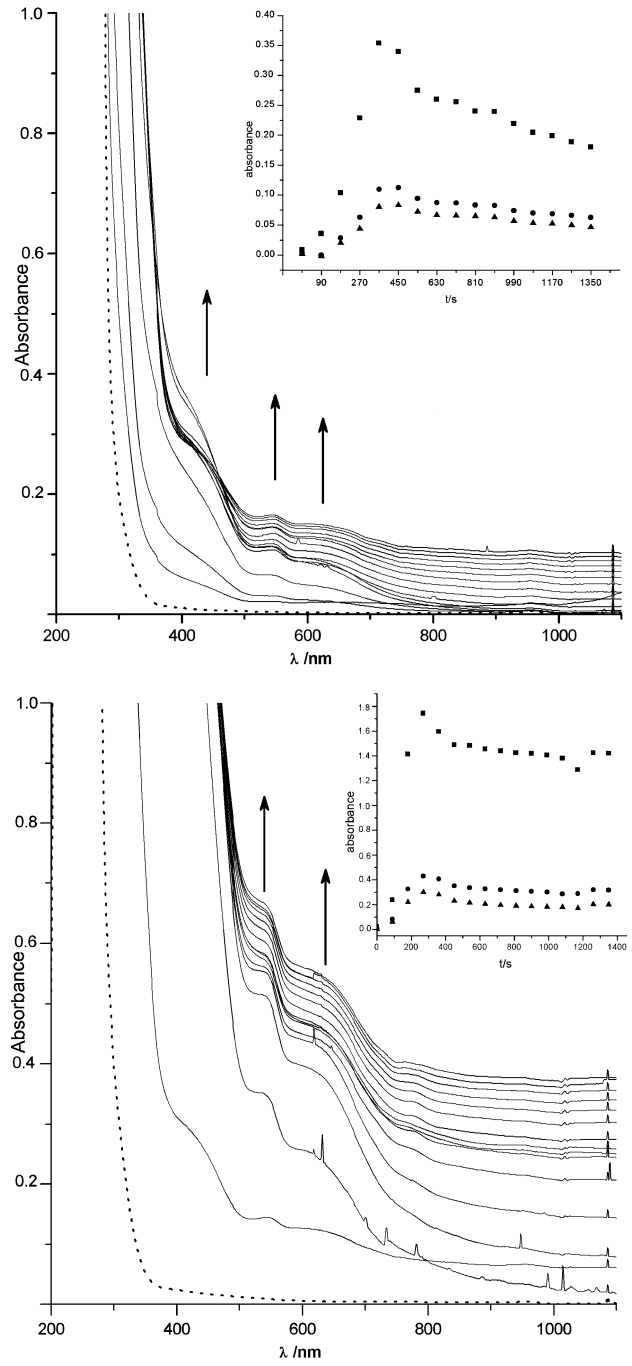

Figure 1. UV−vis spectra of **1** (dotted line) after the addition of H_2O_2: [**1**] = 1×10^{-3} mol·L^{-1}, 3 mL, [H_2O_2] = 6.18 mol·L^{-1}, 10 μL, temperature = 298 K. The spectra were recorded after 90 s incubation. Water was used as solvent. (top) Unbuffered system. (bottom) Buffered system. Insets show the increase and decrease in absorption of the bands at 410 (■), 539 (•), and 620 nm (▲) (unbuffered) and 410 (■), 541 (•), and 630 nm (▲) (buffered) after baseline correction.[33]

(31) Esmelindro, M. C.; Oestreicher, E. G.; Márquez-Alvarez, H.; Dariva, C.; Egues, S. M. S.; Fernandes, C.; Bortoluzzi, A. J.; Drago, V.; Antunes, O. A. C. *J. Inorg. Biochem.* **2005**, *99*, 2054–2061.

(32) Whittaker, M. M.; Barynin, V. V.; Antonyuk, S. V.; Whittaker, J. W. *Biochemistry* **1999**, *38*, 9126–9136.

(33) The baseline offsets arise from dioxygen bubbles in the solution. No precipitation was apparent throughout the course of the reaction. The absorbance values were corrected by employing a baseline correction at 1050 nm.

(34) Gamelin, D.; Kirk, M.; Stemmler, T.; Pal, S.; Armstrong, W.; Penner-Hahn, J.; Solomon, E. *J. Am. Chem. Soc.* **1994**, *116*, 2392–2399.

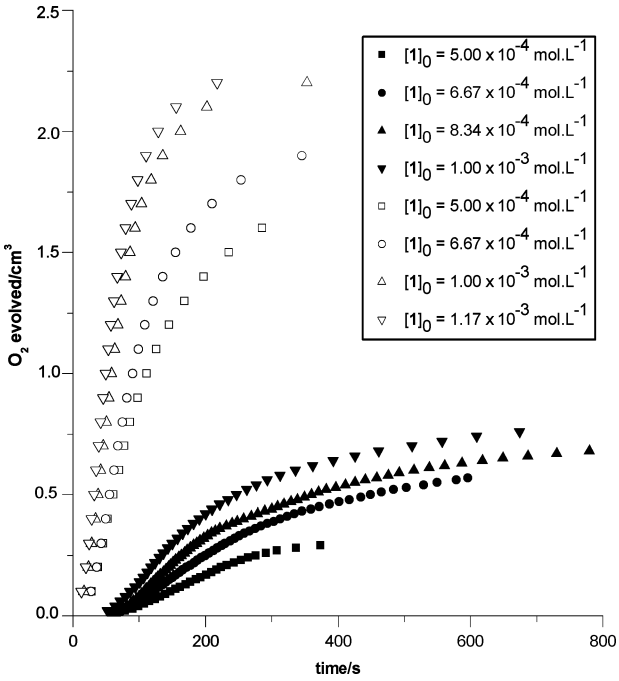

Figure 2. Rates of O_2 evolution at different concentrations of **1**. (filled symbols) Unbuffered solution. (unfilled symbols) Buffered solution. $[H_2O_2] = 7.25 \times 10^{-2}$ mol·L^{-1}.

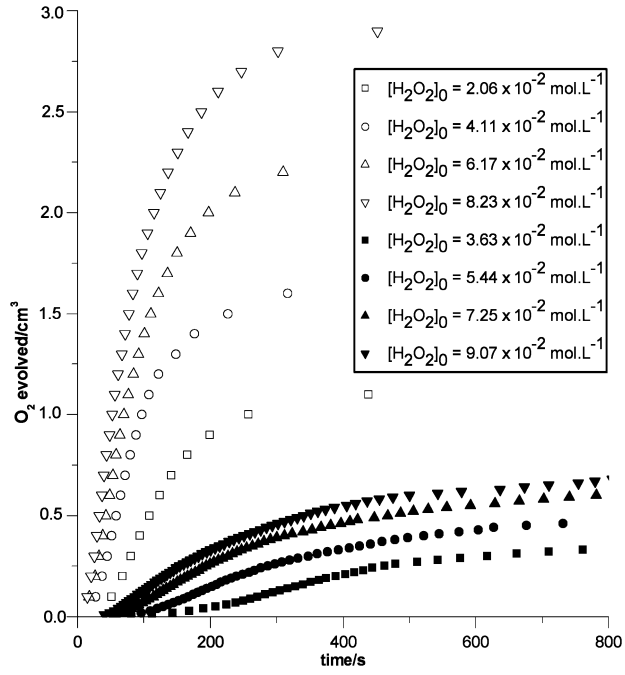

Figure 3. Rates of O_2 evolution at different concentrations of H_2O_2. (filled symbols) Unbuffered solution. (unfilled symbols) Buffered solution. [**1**] = 8.34×10^{-4} mol·L^{-1}.

The reaction between **1** and H_2O_2 was also performed in aqueous solution at constant pH, using a TRIS/TRIS·HCl buffer (pH = 7.2; Figure 2). Similar absorption features were observed but now are about 3−5-fold more intense than in the unbuffered system (i.e., 410, 541, and 630 nm, absorbance = 1.74, 0.43, and 0.30, respectively).[33]

After some time the intensity of the absorption bands decreased in the unbufferred solution but remains more stable in the buffered system (insets in Figure 1-bottom). It is therefore possible that in the unbuffered environment the active species [Mn(III)−(μ-O)$_2$−Mn(IV)] is formed and consumed during the catalytic cycle. Similar behavior was observed for the complex Mn(II)edda reported by Rush and Maskos.[35] Mn(II)edda also forms a Mn(III)−(μ-O)$_2$−Mn(IV) species in the presence of H_2O_2 and the drop in intensity of the absorption bands was attributed to the reaction between Mn(II) and Mn(III)Mn(IV), resulting in Mn(III) species. A similar process may occur with **1** or the degradation of the Mn(IV)−(μ-O)$_2$−Mn(III) core may result from the presence of H^+ ions in solution (vide infra).

Catalase-like Activity and Kinetics of H_2O_2 Disproportionation. The H_2O_2 disproportionation promoted by **1** was investigated in water, at 298 K, by measuring O_2 evolution. The water solubility exhibited by **1** is of relevance since it enables us to study the catalytic reaction under conditions similar to those encountered by MnCATs in a biological environment. Qualitatively, when H_2O_2 is added to an aqueous solution of **1**, the colorless solution turns greenish-brown as O_2 is produced. Gradually, the color changes to yellow and the formation of O_2 decreases. It is worth noting that the catalyst is not able to disproportionate all the H_2O_2 added, which may indicate that the catalytic species is not stable during the process.

The time course of dioxygen evolution is presented in Figures 2 and 3. Owing to the differences in the intensity in the absorption bands observed in the UV−vis spectra for the disproportionation of H_2O_2 promoted by **1** in buffered (pH = 7.2) and unbuffered media (*vide supra*), kinetic experiments were also performed with and without pH control. To determine the rate law of the reaction, the initial rate method was applied. Here, pseudo-first-order kinetic measurements (see the Supporting Information) in unbuffered and buffered solutions indicate that the rate laws are of the form $k_{obs}[complex]^{1.5}[H_2O_2]^{0.7}$ and $k_{obs}[complex]^{1.1}[H_2O_2]^{1.3}$, respectively. Although it is not possible to compare the rates measured under these two different conditions directly, it is evident that in the buffered system oxygen is produced in larger quantity (about 4−6-fold) and more rapidly (Figures 2 and 3). The deviations from first-order dependence of the rate on the concentrations of substrate and complex may be due to the presence of several species of **1** in solution (i.e., mononuclear, dinuclear, and trinuclear).[26] Furthermore, an inspection of the progress curves in Figures 2 and 3 reveal the presence of a small lag phase, which indicates that the active species is formed after H_2O_2 addition.

For several dinuclear manganese catalase biomimetics, a first order dependence of the reaction rate with respect to substrate and catalyst concentration has been observed.[14] Latour and co-workers employed tripodal ligands (tpa, H(bpg), H_2(pda), and H_3(nta))[18] in the preparation of a set of dinuclear di-μ-oxo manganese (Mn(III)Mn(IV) and Mn(II)Mn(III)) compounds with catalase activity. Their results indicated that the disproportionation activity is favored by a lower oxidation state (Mn(III)Mn(III) > Mn(III)Mn(IV)) and by increasing the number of carboxylate groups on the ligand structure (pda > bpg > tpa). They suggested that the higher

(35) Rush, J. D.; Maskos, Z. *Inorg. Chem.* **1990**, *29*, 897–905.

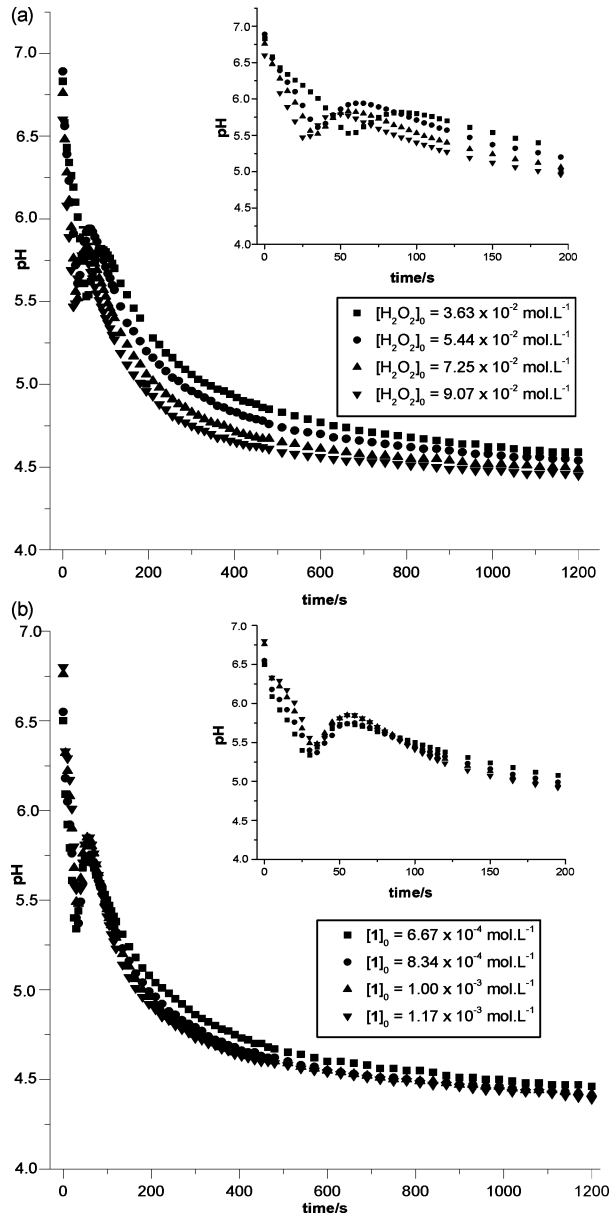

Figure 4. Variation of pH with the progress of the reaction between **1** and H_2O_2: (a) keeping the $[\mathbf{1}] = 8.34 \times 10^{-4}$ mol·L^{-1} constant and (b) keeping the $[H_2O_2] = 8.23 \times 10^{-2}$ mol·L^{-1} constant. The insets show the first 200 s. In a buffered medium, no significant pH variation was observed (data not shown).

activity of compounds containing carboxylate rich ligands might be assigned to the ability of carboxylate groups to act as an internal base, which may indicate that H^+ ions were also released in the reaction of these compounds with H_2O_2. A study of the catalase activity for the compound Mn(edda) revealed that it is inactive below pH 5.15, suggesting that the presence of H^+ ions affect its reactivity. Thus the higher activity presented by **1** in buffered solutions maybe due to the prevention of H^+ inactivation.

Catalase-like Activity and pH Variation. Since it was observed in both electronic absorption and kinetic experiments that the reactivity of **1** is dependent on the pH of the medium, the variation of the pH during H_2O_2 decomposition was monitored.

In the unbuffered system (Figure 4), three distinct steps of pH variation are observed. An initial rapid drop in pH is followed by a transient and rapid increase in pH. Subsequently, a slow exponential pH decrease is recorded. The time related to the first change in pH can be directly correlated to the time of the lag phase observed in the kinetic measurements (Figures 2 and 3), indicating that, during the formation of the active species, protons are released. In the second phase of the pH profile, it is possible to suggest that the protonation of the μ-oxo group leads to a transient increase in pH, while in the third phase the gradual conversion of H_2O_2 to O_2 results in the release of protons. O_2 production stops when the pH reaches 4.5. Since a higher catalytic efficiency is observed (Figures 2 and 3) for **1** when the disproportionation reaction is performed in a buffered system, (pH = 7.2), it is likely that this is a result of the absence of protonation-induced inactivation.

For the reaction between Mn(II)(edda) and H_2O_2, Rush reported a similar variation of pH to that observed for **1** (Figure 4).[35] However, in the Mn(II)(edda) system, the pH turns back returns to the initial values, while for **1** it decreases exponentially.

Interaction of 1 and H_2O_2 by ESI(+)-MS. The gentleness and broadness of ESI and the ability of ESI-MS to provide proper and continuous snapshots of solution constituents have been used extensively by us and others to probe reaction mechanisms involving organic and inorganic species.[36] The ESI(+)-MS spectrum for complex **1** has been previously reported.[26] In a H_2O:MeOH solution (1:1), **1** is at equilibrium with at least four cationic species, which indicates that the single mononuclear solid-state structure of **1** is not totally preserved in solution, since tri-, di-, and mononuclear complexes with compositions $[Mn(II)_3(HPClNOL)_3(NO_3)_5]^+$, $[Mn(II)_3(PClNOL)_2(NO_3)_3]^+$, $[Mn(II)_2(HPClNOL)_2(NO_3)_3]^+$, and $[Mn(II)(HPClNOL)_2(NO_3)]^+$ of *m*/*z* 1348, 931, 878, and 699, respectively, were transferred from solution to gas phase and characterized by ESI(+)-MS/MS.[26] Complex **1** is neutral and could not be detected as such by ESI-(+)-MS.

To probe the mechanism of H_2O_2 disproportionation promoted by **1**, the reaction was monitored by ESI-(+)-MS at room temperature (Figure 5). An appropriate volume of H_2O_2 was added and the resulting reaction solution directly infused into the ESI source of a Q-TOF mass spectrometer. Spectra were recorded before and after (0.2, 3.0, 9.0, and 20 min) the addition of H_2O_2 (Figure 5a−e). Immediately after the addition of H_2O_2, a new ion of *m*/*z* 722 emerges and its abundance increases as a function of reaction time. After 20 min (Figure 5e), the ion of *m*/*z* 722 is still abundant, indicating its substantial stability under these experimental conditions. This species may be assigned as the monocation [(PClNOL)Mn(III)-(μ-oxo)$_2$-Mn(IV)(PClNOL)]$^+$ or [(PClNOL)Mn(II)-(μ-per-

(36) (a) Eberlin, M. N. *Eur. J. Mass Spectrom.* **2007**, *13*, 18–28. (b) Santos, L. S.; Pavam, C. H.; Almeida, W. P.; Coelho, F.; Eberlin, M. N. *Angew. Chem., Int. Ed.* **2004**, *43*, 4330–4333. (c) Raminelli, C.; Prechtl, M. H.; Santos, G. L. S.; Eberlin, M. N.; Comasseto, J. V. *Organometallics* **2004**, *23*, 3990–3996. (d) Santos, L. S; Knaack, L; Metzger, J. O. *Int. J. Mass Spectrom.* **2005**, *246*, 84–104.

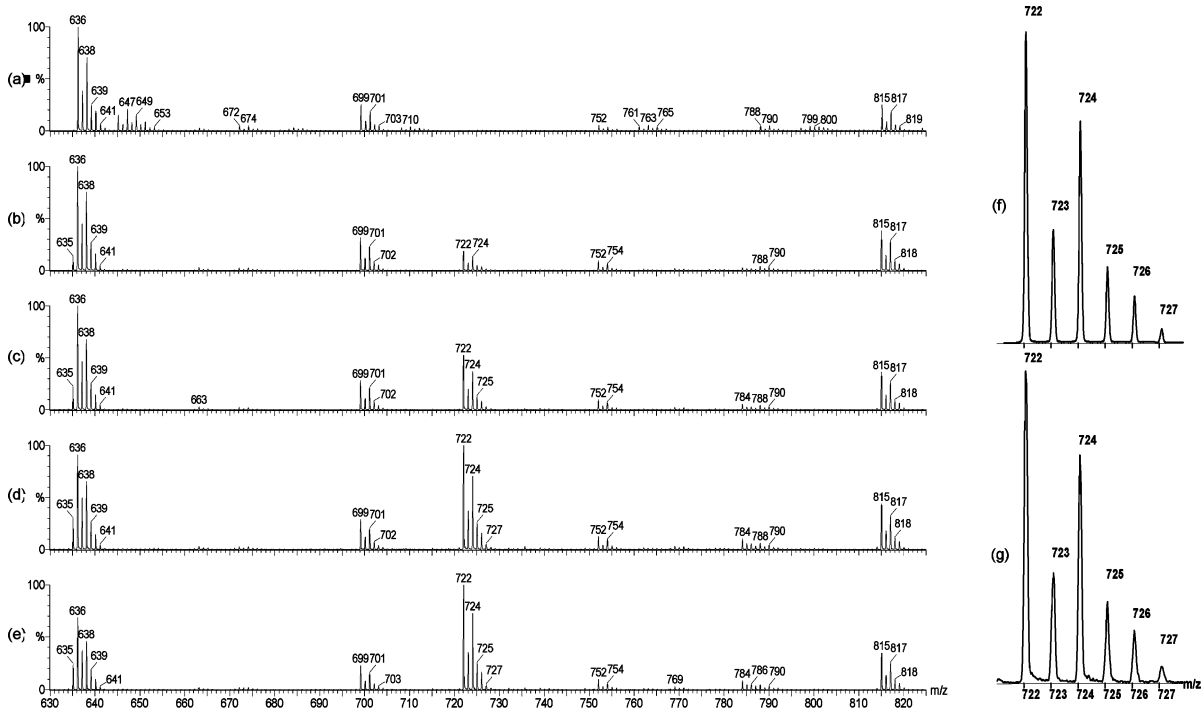

Figure 5. ESI(+)-MS for the reaction in water at 25 °C between **1** and H_2O_2: (a) before H_2O_2 addition; (b) after 0.2 min of H_2O_2 addition; (c) 3 min; (d) 9 min; and (e) 20 min. Insets display the calculated (f) and experimental (g) isotopic patterns for the ion of *m*/*z* 722, that is: [Mn(III)(PClNOL)-(μ-oxo)$_2$-Mn(IV)(PClNOL)]$^+$ = $Mn_2C_{30}H_{34}N_6O_4Cl_2$.

oxo)-Mn(III)(PClNOL)]$^+$, but a di-μ-oxo-Mn(III)Mn(IV) instead of μ-peroxo-Mn(II)Mn(III) species is supported by UV−vis and EPR (*vide infra*).

The assignment of the ion of *m*/*z* 722 is in good agreement with intermediates previously proposed for other dinuclear manganese complexes that show catalase-like activity.[21] Since this species is formed immediately after the addition of H_2O_2 to **1**, the formation of the di-μ-oxo species is expected to be associated with the H_2O_2 disproportionation that forms a stable Mn(III)−(μ-O)$_2$−Mn(IV) intermediate. Note that although **1** in the solid state is mononuclear, it appears to form the same heterovalent core (Mn(III)−(μ-O)$_2$−Mn(IV)) as observed when the dinuclear compound [Mn(II)$_2$(L)(OAc)$_2$(CH$_3$OH)](ClO$_4$) was allowed to react with H_2O_2.[21]

Interaction of 1 with H_2O_2 by EPR. The reactivity of **1** toward H_2O_2 was also investigated by measuring changes in the EPR spectra at two different H_2O_2 concentrations. The EPR spectrum of **1** ([**1**]$_{final}$: 9.57 × 10^{-4} mol·L^{-1}) in TRIS/HCl (pH 7.2) buffer solution at 140 K is shown in Figure 6a. This spectrum has broad features at low field, $g_{eff} \sim 5$ and $g_{eff} \sim 3$, and a broad feature at $g_{eff} = 2$ that are characteristic of a dinuclear Mn(II)Mn(II) species described by the groups of Pecoraro[17] and Dubois.[18,21] After the addition of H_2O_2 at a low concentration ([H_2O_2]$_{final}$ = 2.34 × 10^{-2} mol·L^{-1}; Figure 6b) to **1** the spectrum changes with the appearance of a typical 16-line signal centered around $g = 2$ that is attributed to a Mn(IV)Mn(III) species.[17,18,21] With the addition of H_2O_2 at higher concentrations ([H_2O_2]$_{final}$ = 1.87 × 10^{-1} mol·L^{-1}; Figure 6c), the 16-line spectrum increases in intensity and the Mn(II)Mn(II) spectrum disappears. After the addition of a second aliquot of H_2O_2 ([H_2O_2]$_{final}$ = 3.74 × 10^{-1} mol·L^{-1}), the spectrum changes with the partial loss of the 16-line signal and the appearance of a new signal at $g = 2$ with a six-line Mn hyperfine structure ($A/g\beta \sim 8.9$ mT), characteristic of an isolated mononuclear Mn(II) species (Figure 6d). With the addition of a third aliquot of H_2O_2 ([H_2O_2]$_{final}$ = 5.61 × 10^{-1} mol·L^{-1}; Figure 6e), the 16-line spectrum was completely absent and the only species seen by EPR is mononuclear Mn(II). At each point in the titration, the sample was thawed and incubated at 45 °C for several minutes but no further changes to the EPR spectra were observed.

The spin Hamiltonian for a dinuclear heterovalent Mn(III)-Mn(IV) center (eq 1) incorporates electron Zeeman, fine structure and Mn hyperfine coupling terms for each ion and the isotropic and anistropic exchange coupling.

$$H = -2J_{iso}S_1S_2 + S_1JS_2 + \sum_{j=1}^{2} \beta B g_j S_j + S_j D_j S_j + S_j A_{Mnj} I_{Mnj} - g_n \beta_n B I_{Mnj} \quad (1)$$

Since the antiferromagnetic exchange coupling in a di-μ-oxo bridged species is extremely large ($|-2J_{iso}| > 100$ cm^{-1}) with $|J_{iso}| > |D|$, the spin states (S_T) can be described by $S_T = |S_1 + S_2|, |S_1 + S_2 - 1|,..., |S_1 - S_2|$ (i.e., S_T = 1/2, 3/2, 5/2, 7/2) in the strong exchange regime. Consequently at low temperatures only the $S_T = 1/2$ spin state will be populated. Computer simulation of the 16-line EPR spectrum (Figures 6c and 7a) was performed with the following spin Hamiltonian for an $S = 1/2$ coupled representation:

$$H = \beta B g S + S A_{Mn(III)} I_{Mn(III)} - g_n \beta_n B I_{Mn(III)} + S A_{Mn(IV)} I_{Mn(IV)} - g_n \beta_n I_{Mn(IV)} \quad (2)$$

having the following g and A(Mn) matrices: $g_x = 2.0014$, $g_y = 2.0030$, $g_z = 1.9865$, $A(\mathrm{Mn(III)})_x = 136.3 \times 10^{-4}$

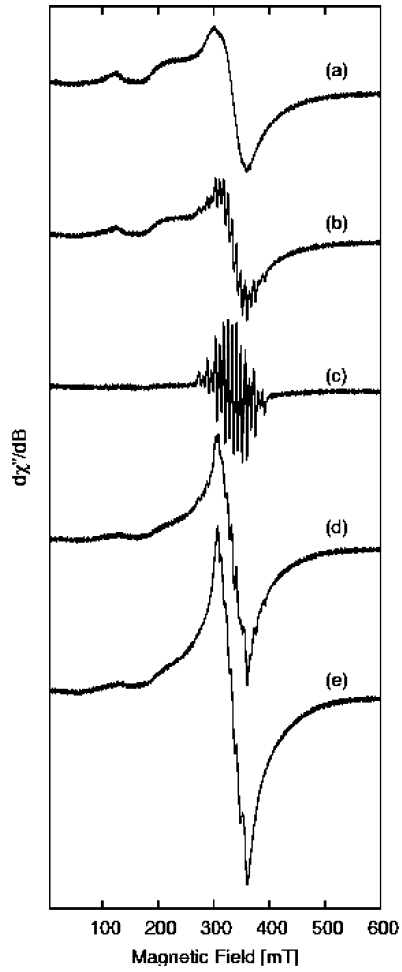

Figure 6. X-band EPR spectra of **1** at 140 K in a buffered solution, ν = 9.34854 GHz: (a) **1** prior to the addition of H_2O_2 ([**1**]: 1.0×10^{-3} M), (b) frozen immediately after the addition of 1.8% H_2O_2 ($[H_2O_2]_{final} = 2.34 \times 10^{-2}$ M), (c) frozen immediately after the addition of 8 μL of 15% H_2O_2 ($[H_2O_2]_{final} = 1.87 \times 10^{-1}$ M), (d) a second aliquot (8 μL) of 15% H_2O_2 ($[H_2O_2]_{final} = 3.74 \times 10^{-1}$ M) was added to sample c and frozen after 2 min incubation, (e) a third aliquot (8 μL) of 15% H_2O_2 ($[H_2O_2]_{final} = 5.61 \times 10^{-1}$ M) was added to sample d and frozen after 2 min incubation.

cm^{-1}, $A(Mn(III))_y = 155.5 \times 10^{-4}$ cm^{-1}, $A(Mn(III))_z = 103.4 \times 10^{-4}$ cm^{-1}, $A(Mn(IV))_x = 75.3 \times 10^{-4}$ cm^{-1}, $A(Mn(IV))_y = 68.6 \times 10^{-4}$ cm^{-1}, $A(Mn(IV))_z = 77.4 \times 10^{-4}$ cm^{-1}. The resulting simulation (Figure 7b) is in excellent agreement with the experimental spectrum. The spin Hamiltonian parameters obtained from the simulation are similar to those for other Mn(III)Mn(IV) species reported in the literature.[37]

Mechanistic Implications for the Catalase-like Reactivity of 1. On the basis of the kinetic, spectroscopic and spectrometric data presented herein and mechanistic models described previously,[13,14c,f,15a,20,21] a scheme for the reaction mechanism employed by **1** is proposed (Figure 8). Importantly, at room temperature, there is no evidence for the involvement of free radicals. The proposed model accounts for the experimentally observed species, including the formation of a Mn(III)−(μ-O)$_2$−Mn(IV) intermediate, oxygen evolution, and the observed pH changes in unbuffered reactions.

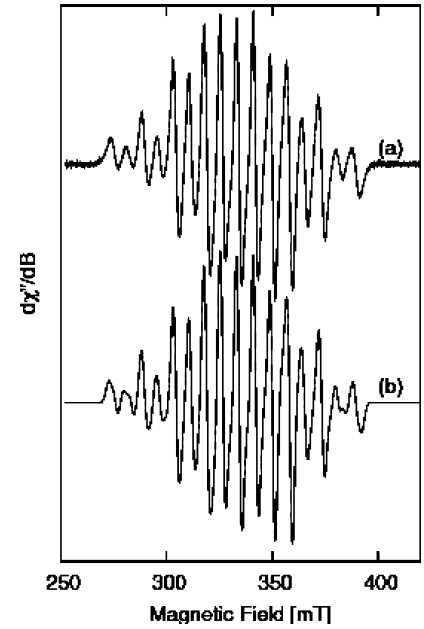

Figure 7. X-band (ν = 9.34854 GHz) EPR spectrum of **1** at 140 K in a buffered solution (pH 7.2): (a) experimental spectrum of complex **1** frozen immediately after the addition of 8 μL of 15% H_2O_2 ($[H_2O_2]_{final} = 1.87 \times 10^{-1}$ M), (b) computer simulation; see text for details.

In the initial phase, there is an equilibrium between the mono-, di-, and trinuclear forms of **1**,[26] with the dimeric form being predominant in buffered solutions as reflected in the EPR spectra (Figure 6). Reaction of 2 molecules of **1** (Mn(II)−Mn(II)) and two molecules of H_2O_2 produces two molecules of complex A with a Mn(III)−(μ-O)$_2$−Mn(III) core. Subsequently, in the presence of H_2O_2, a "dimer-of-dimers" species (complex B) is formed with a di-μ-oxo group as a bridge between the two dimanganese complexes. Concomitant with the formation of this interdimer di-μ-oxo bridge is the oxidation of Mn(III) to Mn(IV). Thus, the first step in the formation of this tetramer should be the formation of an interdimer peroxide bridge, as proposed previously by Ōkawa.[38] A similar tetranuclear manganese compound containing three di-μ-oxo units was published previously.[39] The proposed release of protons associated with the formation of species A and B contributes to the initial drop in pH observed in the unbuffered reactions (Figure 4). The decomposition of complex B results in the formation of the mixed-valence complex with a Mn(III)−(μ-O)$_2$−Mn(IV) core (complex C) and release of H_2O. The experimental (EPR and ESI-(+)-MS) observation of this mixed valence species indicates that this is an intermediate in the reaction mechanism and, further, that the rate determining step (protonation of species C to yield species D) occurs after its formation. The very low pK_a of the doubly Lewis activated μ-oxo bridge and the observation that the time

(37) Schäfer, K. O.; Bittl, R.; Lendzian, F.; Barynin, V.; Weyhermüller, T.; Wieghardt, K.; Lubitz, W. *J. Phys. Chem. B.* **2003**, *107*, 1242–1250.

(38) Wada, H.; Motoda, K.; Ohba, M.; Sakiyama, H.; Matsumoto, N.; Ōkawa, H. *Bull. Chem. Soc. Jpn.* **1995**, *68*, 1105–1114.

(39) Philouze, C.; Blondin, G.; Menuge, S.; Auger, N.; Girerd, J.-J.; Vigner, D.; Lance, M.; Nierlich, M. *Angew. Chem., Int. Ed.* **1992**, *31*, 1629–1631.

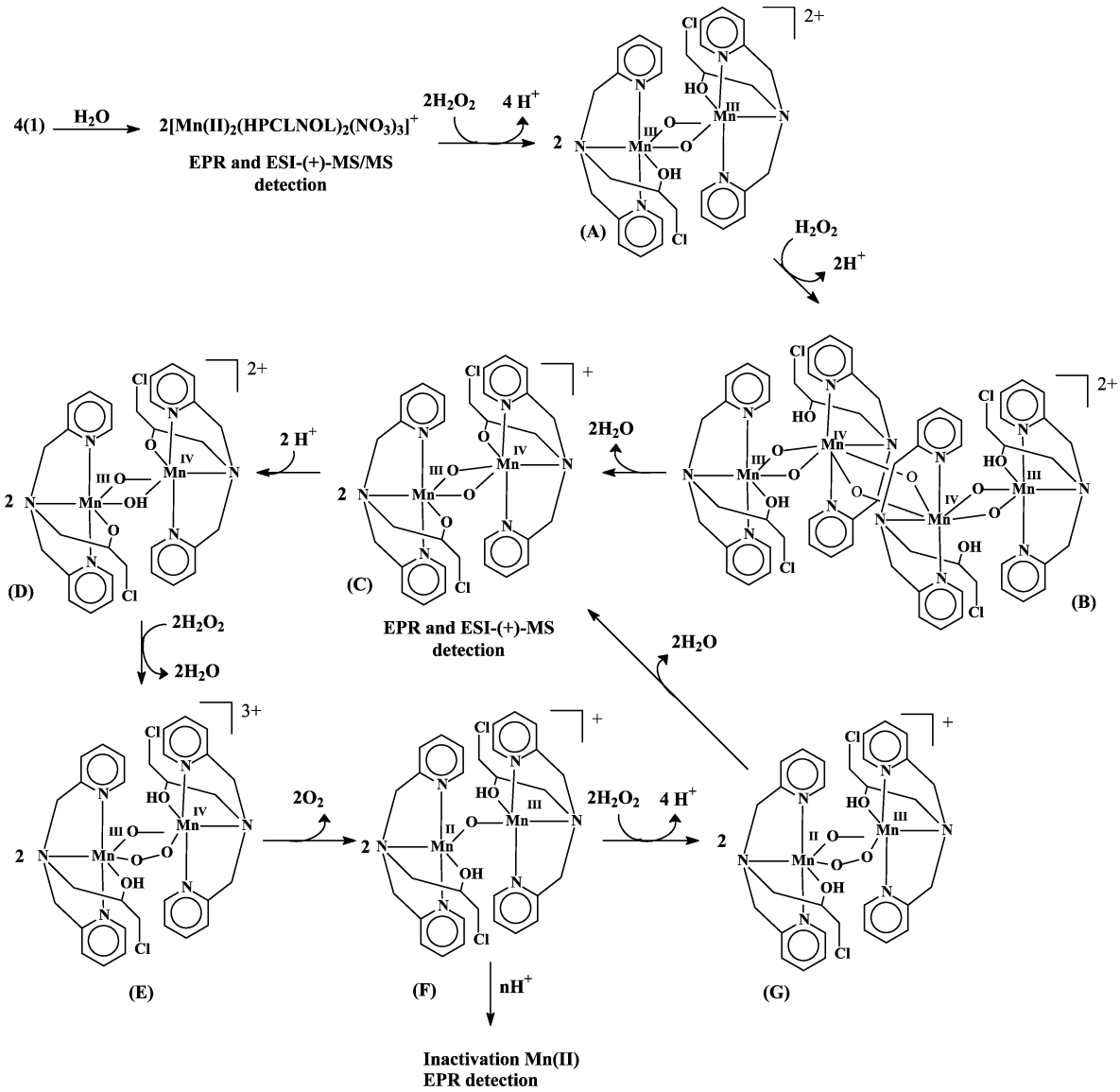

Figure 8. Mechanistic proposal for the H_2O_2 disproportionation reaction promoted by **1** based on the EPR, ESI-(+)-MS, and pH variation results.

span from mixing **1** and peroxide to the formation of species C accounts exactly for the observed lag in O_2 evolution (Figures 2 and 3) are also consistent with the rate determining step being the protonation of the μ-oxo bridge in species C. Thus, accumulation of species C and protons leads to a burst of proton consumption with a concomitant rise in pH (Figure 4) and formation of species D. Subsequently, complex D reacts with H_2O_2 (μ-η^1:η^1 coordination) forming complex E, which releases O_2, generating complex F. The coordination of a further H_2O_2 molecule to complex F results in the release of H^+ ions and formation of species G. This species undergoes H_2O elimination with concomitant two-electron oxidation of the Mn(II)Mn(III) core (complex G), leading to the formation of the experimentally observed [(PClNOL)-Mn(III)(μ-O)$_2$Mn(IV)(PClNOL)]$^+$ (complex C) intermediate again completing the catalytic cycle (species C−G). Importantly, there is a net release of protons in the catalytic cycle which leads to the gradual decrease of pH over the time course of the reaction (Figure 4). The EPR studies revealed that a mononuclear Mn(II) species is obtained after incubation with excess of H_2O_2 (Figure 6d and e). This observation is interpreted in terms of an inactivation of the catalytic complex F by protonation of the oxo bridge or ligand molecule (below pH 4.5, the complex is inactive). The gradual inactivation of complex F results in decreased dioxygen evolution (Figures 2 and 3), decreased amounts of species C (Figure 6), and incomplete consumption of hydrogen peroxide, all of which are observed experimentally. Similar inactivation at low pH has been observed previously,[14d,40−44] and consequently, the proposed reaction mechanism should be considered pseudo-catalytic.

(40) Pal, S.; Armstrong, W. H. *J. Am. Chem. Soc.* **1992**, *114*, 6398–6406.
(41) Cooper, S. R.; Calvin, M. *J. Am. Chem. Soc.* **1997**, *99*, 6623–6630.
(42) Pal, S.; Armstrong, W. H. *Inorg. Chem.* **1992**, *31*, 5417–5423.
(43) Sarneski, J. E.; Didiuk, M.; Thorp, H. H.; Crabtree, R. H.; Brudvig, G. W.; Faller, J. W.; Chullte, G. K. *Inorg. Chem.* **1991**, *30*, 2833–2835.
(44) Pal, S.; Olmstead, M. M.; Armstrong, W. H. *Inorg. Chem.* **1995**, *34*, 4708–4715.

Table 1. Results for the Cyclohexane Oxidation Catalyzed by **1** after 24 h[a]

				yield (%)[b]							
entry	T (°C)	oxidant	solvent	CyOH	Cy=O	Cy−OOH	Cy−OO*t*-Bu	AA	total	CyOH/Cy=O	TN[c]
1	rt	H_2O_2	MeCN					0.13	0.13		1.3
2	50	H_2O_2	MeCN	1.3	1.0	3.8		0.13	6.2	1.3	62.3
3	rt	*t*-BuOOH	MeCN			0.5		0.14	0.63		6.3
4	50	*t*-BuOOH	MeCN	8.9	15	0.21	4.4	0.16	28.7	0.59	286.7
5	rt	H_2O_2	*t*-BuOH					0.2	0.2		0.2
6	50	H_2O_2	*t*-BuOH	0.49	0.35	1.0		0.16	2	1.4	20
7	rt	*t*-BuOOH	*t*-BuOH	0.35	0.74	1.2	0.29	0.13	2.7	0.47	27.1
8	50	*t*-BuOOH	*t*-BuOH	7.1	13.7	0.8	3.8	0.85	26.2	0.52	262.5

[a] Ratio catalyst:substrate:oxidant = 1:1000:1000. [b] $R_{rc} = (R_c \times n_c)/n_t$; $R_t = R_{AA} + (R_c \times n_c)/n_t$; R_{rc} = corrected chromatographic yield; R_c = chromatographic yield; $n_c = n_t - n_{aa}$; R_{aa} = adipic acid yield. [c] TN = turnover number; calculated as moles of products per mole of catalyst.

Scheme 2. Products of the Cyclohexane Oxidation Performed by **1**

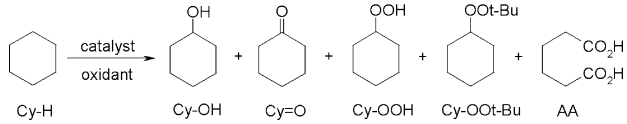

Oxidation of Cyclohexane by 1. H_2O_2 disproportionation is catalyzed by catalases. These enzymes may be regarded as a special example of peroxidases in which the substrate oxidized by H_2O_2 is another molecule of H_2O_2.[45] Conversely, typical peroxidases use H_2O_2 to perform oxygenations of various substrates.[3] Thus, peroxidases have been characterized as heme containing proteins that catalyze the oxidation of particular organic compounds using H_2O_2 as an electron acceptor. Catalase and peroxidase activities have been corroborated with other manganese compounds.[46−48] For the manganese complex to act as an oxidation catalyst, it is required that the oxidized state of the catalyst oxidizes the organic substrate instead of oxidizing H_2O_2.[46]

We have thus investigated whether **1** may also utilize peroxide (H_2O_2, *t*-BuOOH) molecules in an alternative reaction pathway, namely the oxidation of cyclohexane.

Cyclohexanol (Cy−OH), cyclohexanone (Cy=O), cyclohexyl hydroperoxide (Cy−OOH), *tert*-butyl cyclohexyl peroxide (Cy−OOt−Bu), and adipic acid (AA) were formed (Table 1) during the oxidation process (Scheme 2). The greatest yield was obtained when *t*-BuOOH was used as an oxidant at 50 °C (experiments 4 and 8 in Table 1). The effect of solvent (acetonitrile or *t*-BuOH) was negligible. With H_2O_2 as oxidant, very low product yields were obtained (experiments 1, 2, 5, and 6 in Table 1). Thus, whereas the reaction between **1** and H_2O_2 is bifunctional, the disproportionation reaction is preferred. In contrast, *t*-BuOOH appears to be a suitable substrate for performing oxygenation reactions with **1**. Recently, we have analyzed the oxidation of cyclohexane with H_2O_2 and *t*-BuOOH as oxidant, using a family of mononuclear iron(III) compounds with similar ligands (*i.e.* $[Fe(BMPA)Cl_3]$, $[Fe(MPBMPA)Cl_3]$, $[Fe(PBMPA)Cl_2]$, and $[Fe(PABMPA)Cl_2]^+$).[49,50] In contrast to **1**, cyclohexane oxidation in the presence of these iron compounds is more efficient when H_2O_2 is employed as the oxidant. Especially for $[Fe(PABMPA)Cl_2]^+$, for which we have also characterized their catalase activity,[50] the yield obtained in the cyclohexane oxidation with H_2O_2 was 33.4% as compared to a marginal 5.4% yield when *t*-BuOOH was employed. For these iron compounds, Cy−OOH and Cy−OO*t*-Bu were identified as products of the cyclohexane oxidation, suggesting the operation of a Fenton or Haber−Weiss mechanism.[51,52]

The lack of cyclohexyl peroxides as products in the reactions between **1** and H_2O_2 at room temperature indicates that no radical species are formed under these conditions. The identification of Cy−OOH at 50 °C shows, however, that a side reaction other than H_2O_2 disproportionation is taking place under this condition. When *t*-BuOOH was used as an oxidant, a larger amount of alkyl peroxide was identified as the product with no O_2 production, suggesting that the interaction between *t*-BuOOH and **1** forms radical species.

Conclusions

We have shown that a Mn(II) complex, which is mononuclear in the solid state, is capable of promoting H_2O_2 disproportionation in aqueous solution, and that a relatively stable Mn(III)−(μ-O)$_2$−Mn(IV) intermediate is formed during the course of the reaction. Three steps of pH variation (two deprotonations and one protonation) were observed for H_2O_2 disproportionation by **1**, which are directly involved in the formation of the Mn(III)−(μ-O)$_2$−Mn(IV) active species and in the inactivation of the catalyst, which occurs near pH 4.5. Larger amounts of O_2 are produced in a buffered medium (pH 7.2) than in unbuffered medium, and this observation supports the hypothesis that the main pathway for catalyst inactivation is *via* protonation. The low yield of cyclohexane oxidation when H_2O_2 was used as oxidant versus *t*-BuOOH indicates that **1** acts mainly as a catalase rather than a peroxidase mimic.

(45) Reddy, K. H. *Bioinorganic Chemistry*; New Age International Publishers: New Delhi, 2006.
(46) Boer, J. W.; Browne, W. R.; Feringa, B. K.; Hage, R. *C. R. Chim.* **2007**, *10*, 341–354.
(47) Shul'pin, G. B. *J. Mol. Catal. A: Chem.* **2002**, *189*, 39–66.
(48) Woitiski, C. B; Kozlov, Y. N.; Mandelli, D.; Nizova, G. V.; Schuchardt, U.; Shul'pin, G. B. *J. Mol. Catal. A: Chem.* **2004**, *222*, 103–119.
(49) Carvalho, N. M. F.; Horn, A.; Antunes, O. A. C. *Appl. Catal., A* **2006**, *305*, 140–145.
(50) Carvalho, N. M.F.; Horn, A.; Bortoluzzi, A. J.; Drago, V.; Antunes, O. A. C. *Inorg. Chim. Acta* **2006**, *359*, 90–98.
(51) Fenton, H. J. H. *J. Chem. Soc.* **1894**, *65*, 899–910.
(52) Haber, F.; Weiss, J. *Naturwissenschaften* **1932**, *51*, 948–950.

Acknowledgment. J.A.L., É.S.B., A.H., Jr., O.A.C.A., and C.F. are grateful for grants from FAPERJ, CAPES, CNPq, and PRONEX. M.B., R.R.C., and M.N.E. are grateful for grants from FAPESP and CNPq. G.S. and G.R.H. acknowledge financial support from the Australian Research Council.

Supporting Information Available: Differential pulse voltammogram and kinetic plots. This material is available free of charge via the Internet at http://pubs.acs.org.

IC801969C